frontiers | Frontiers in Environmental Chemistry

TYPE Original Research
PUBLISHED 29 May 2024
DOI 10.3389/fenvc.2024.1375705

OPEN ACCESS

EDITED BY
Benton Otieno,
Vaal University of Technology, South Africa

REVIEWED BY
Stephen Otieno,
Maseno University, Kenya
Saheed Olalekan Sanni,
University of Pretoria, South Africa

*CORRESPONDENCE
Pierre Gerard Tchieta,
pgtchieta@yahoo.fr

RECEIVED 26 January 2024
ACCEPTED 08 April 2024
PUBLISHED 29 May 2024

CITATION
Ndongmo JN, Mabou JL, Tchuifon Tchuifon DR, Makota S, Fotsop CG, Conde M and Tchieta PG (2024), Synthesis and characterization of peanut shell-derived ferromagnetic activated carbon: application in the Fenton process for the degradation of methyl orange.
Front. Environ. Chem. 5:1375705.
doi: 10.3389/fenvc.2024.1375705

Synthesis and characterization of peanut shell-derived ferromagnetic activated carbon: application in the Fenton process for the degradation of methyl orange

Josiane Nguimatsia Ndongmo[1], Jules Leuna Mabou[1], Donald Raoul Tchuifon Tchuifon[2,3], Suzanne Makota[1], Cyrille Ghislain Fotsop[4], Miriame Conde[1] and Pierre Gerard Tchieta[1]*

[1]Department of Chemistry, Faculty of Science, University of Douala, Douala, Cameroon, [2]Department of Chemistry, Research Unit of Noxious Chemistry and Environmental Engineering, Faculty of Science, University of Dschang, Dschang, Cameroon, [3]Department of Process Engineering, Laboratory of Energy, Materials, Modeling and Method, National Higher Polytechnic School of Douala, University of Douala, Douala, Cameroon, [4]Institute of Chemistry, Faculty of Process and Systems Engineering, Universität Platz, Magdeburg, Germany

The objective of the current work was to synthesize and characterize ferromagnetic activated carbon from peanut shells (PSs) and apply it for the degradation of methyl orange (MO) following the heterogeneous Fenton process. PSs were activated with phosphoric acid and potassium hydroxide at 1:1, 1:2, and 1:3 solid/liquid activation ratios and different concentrations (0.5, 1, and 1.5 M) and pyrolized at 500°C. Based on the iodine indexes, KOH-activated carbon adsorbents exhibited higher porosity than the H_3PO_4-activated adsorbents. KOH-activated carbon at a 1:3 activation ratio (iodine value 591 mg/g) was selected for magnetization using iron (II) ions and catalytic mineralization of MO dye. The ferromagnetic activated carbon (AC-PS@FeII) was characterized using Fourier-transform infrared (FTIR) spectroscopy, X-ray diffraction (XRD), scanning electron microscopy (SEM), energy-dispersive X-ray (EDX) analysis, and nitrogen-adsorption BET measurements. AC-PS@FeII contained ferromagnetite with a cubic spinel structure and a specific area of 181.96 $m^2 \cdot g^{-1}$. AC-PS@FeII degraded MO with a degradation efficiency of 99.22% at pH 2, 4 g/L of catalyst dosage, and a 50-min contact time. The results of recyclability tests, using distilled water, revealed a slight decrease in degradation capacity after four runs, indicating that the developed catalyst was appreciably stable. The hetero-Fenton catalyst from peanut shells could be an ideal catalyst for treating wastewater contaminated with dyes as a path toward a circular economy.

KEYWORDS

ferromagnetic activated carbon, methyl orange, Heterogeneous Fenton, peanut shells, pyrolysis

1 Introduction

Dye pollution has become a widespread environmental problem because of its wide application in industries such as the paper, textiles, plastic, and leather tanning industries in the past several decades (Bernardi et al., 2010; Dong et al., 2017). Over 100,000 commercial dyes are produced annually at an estimated annual production rate of over 800,000 tons (Couture et al., 2013). Large amounts of dye-containing effluents pose a great threat to the environment because of their strong color, complex structure, stability, and low biodegradability (Du et al., 2016). Therefore, it is of vital importance to remove dyes from wastewater to protect aquatic and terrestrial lifeforms and minimize the hazards associated with water pollution.

Unlike physical and biological treatment methods, chemical oxidation methods such as homogeneous and heterogeneous Fenton treatment methods are capable of mineralizing a wide range of organic pollutants (Varjani and Sudha, 2018). However, compared to the homogeneous Fenton process, the easy recovery of the exhausted catalyst after application in the case of a heterogeneous Fenton process makes it more convenient (Cuerda-Correa et al., 2020). Following that, many researchers have reported various methods of enhancing the efficiency of a heterogeneous Fenton process. A common method involves immobilizing the metallic ions/oxides onto various supports to maximize the synergistic effect of the catalytic and adsorptive properties of the additive oxide and the host material (Shikuku et al., 2018). Such supports, including activated carbon (Jaafarzadeh et al., 2015), carbon nanotubes (Cleveland et al., 2014), graphite oxide (Cleveland et al., 2014), and SBA-15 (Hua et al., 2014), are capable of improving the efficiency of the Fenton process by scavenging the pollutant and also easing the catalyst recovery process after application. The inherent limitations of homogeneous catalysis attract high capital investment for industrial use in wastewater treatment, particularly in developing countries. This could be navigated using heterogeneous Fenton catalysis involving immobilization of largely abundant iron oxide-based catalysts on a low-cost porous solid support. Hydroxyl radicals are produced from the catalytic decomposition of H_2O_2 by ferrous or ferric salts (Zhou et al., 2019). This process uses relatively inexpensive and non-toxic reactants and catalysts and shows great potential for industrial applications.

Activated carbon prepared from waste biomass such as peanut shells (PSs) (abundant in Cameroon and other regions of Africa) by chemical activation has gained widespread interest (Wang et al., 2020; Fletcher et al., 2024). Additionally, the utilization of otherwise waste materials is consistent with the principles of a circular economy (Ngeno et al., 2022). The use of readily available and non-exhaustible biomass, such as peanut shells, that can be easily and cost-effectively transformed into high-surface area adsorbents and catalyst support materials for iron impregnation is attractive. Moreover, their valorization contributes toward solving the problem of solid waste disposal in many communities. Subsequently, the hydrothermal method was used for the precipitation of iron oxide into the activated carbon matrix. The development of activated carbons functionalized with active iron oxide phases for the Fenton reaction is a promising way to obtain new multifunctional porous materials combining adsorption and advanced oxidation, allowing the development of an efficient, economical, and environmentally friendly treatment process (Joshi et al., 2012; Ngueabouo et al., 2022). The control of the properties of the host material is important to optimize the functionality of the composite catalyst. The properties of activated carbon depend on the type of biomass, activation method (chemical or thermal), identity of the chemical activators (gas, acid, alkali, and salt), concentration of the activator agent, precursor-to-activator ratio, and pyrolysis conditions (temperature and residence time) (Chimi et al., 2022; Njewa and Shikuku, 2023; Taquieteu et al., 2023). Furthermore, the surface chemistry and performance of the metal oxide–carbon composite are also governed by the identity of the metal oxide(s) and the fraction by mass (Jacques et al., 2023). The complexity of the interactions between these variables implies that the properties of the activated carbon cannot be predicted *a priori* and must be optimized empirically for a particular biomass type. Such optimization would be cumbersome and expensive. A response surface methodology (RSM) provides a convenient tool for the optimization of adsorbent properties when the input variables (process conditions) are known (Sidjou et al., 2023). Therefore, the textural properties, surface chemistry, and catalytic performance of peanut shell-derived ferromagnetic activated carbon as Fenton catalysts for the mineralization of methyl orange are unknown. The objective of the present work was to (i) determine the activator agent (acid or alkali) and activation conditions (precursor-to-activator ratio and concentration of activator) that provide a maximized porosity structure for peanut shell-derived-activated carbons using RSM design and (ii) prepare a ferromagnetic activated carbon for the Fenton-type degradation of methyl orange (MO) under optimized process conditions. Of special interest was the study of the textural properties, surface chemistry, and catalytic performance.

2 Materials and methods

2.1 Materials and chemicals

Peanut shells were collected in the town of Dschang, Menoua Department, West Region of Cameroon. Subsequently, the peanut shells were washed and rinsed several times with distilled water, dried in the sun, and then crushed and sieved through a 100-μm sieve. Iron sulfate heptahydrate ($FeSO_4.7H_2O$, purity 99%) and sodium hydroxide (NaOH, purity 97%) were acquired from Fisher Scientific, and hydrogen peroxide (H_2O_2, 50%) and MO (98%) of chemical formula $C_{14}H_{14}N_3O_3S^-Na^+$ were purchased from Prolado.

2.2 Preparation of activated carbons

The activated carbons from peanut shells were prepared by the chemical activation of the biomass using activating agents H_3PO_4 and KOH at different concentrations (0.5 M, 1 M, and 1.5 M) using varying precursor-to-activator (S/L) ratios (1:1, 1:2, and 1:3). A mass of 120 g of the materials was immersed in 150 mL of activating agent solution. The mixtures were stirred for 30 min and then oven-dried at 105°C for 48 h. The activated samples were carbonized for 1 h at 500°C at a heating rate of 5°C/min under inert conditions. The pyrolysis products (carbons) were washed several times with

distilled water until the effluent attained neutral pH. The activated carbon pastes were oven-dried at 105°C for 24 h, crushed into powder, and then sieved through a 100-µm sieve. The relative porosity structures of the activated carbons were characterized by the iodine index method (Kuete et al., 2018).

2.3 Magnetization of activated carbon

The magnetically responsive activated carbon composites were prepared following the hydrothermal method. In brief, 10 g of previously prepared activated carbon was introduced into 250 mL of an aqueous solution containing 5 g of NaOH and 30 g of $FeSO_4.7H_2O$ under magnetic stirring at 80°C for 2 h. The resulting mixture was then filtered, and the residue was washed several times with distilled water until pH of the supernatant matched pH of the initial distilled water. The residue was then oven-dried at 105°C for 24 h to obtain ferromagnetic activated carbon (Cuerda-Correa et al., 2020).

2.4 Characterization of activated carbon and magnetic activated carbon

Fourier-transform infrared spectroscopy (FTIR) spectra were obtained using a Genesis FTIR Spectrometer (Bruker Optics GmbH, Rudolf-Plank-Str. 27, 76275 Ettlingen, Germany) (Mattson ATI) equipped with a deuterated triglycine sulfate (DTGS) detector in the transmission mode from 400 to 4,000 cm^{-1} after 20 scans.

X-ray diffraction (XRD) data were collected on a STOE STADI P powder diffractometer (Stoe & CIE GmbH, Darmstadt, Germany) with Cu-Kα1 radiation (λ = 1.54056 Å; Ge monochromator; flat samples) in transmission geometry using a DECTRIS® MYTHEN 1 K detector (DECTRIS, Baden-Daettwil, Switzerland).

The surface morphology of the materials was inspected using scanning electron microscopy (SEM)/energy-dispersive X-ray (EDX) analysis and field emission scanning electron microscopy coupled with energy-dispersive X-ray microanalysis (FE-SEM/EDX) using a Magellan 400-L scanning electron microscope.

The specific surface area, pore size, and pore volume of the three materials were determined from N_2 adsorption and desorption using the BET/BJH models using a BELSORP MAX apparatus from Bel Japan Inc. The sorption experiments were carried out at 77 K.

2.5 Fenton oxidation experiments using the synthesized catalyst

The RSM based on the centered composite design (CCD) was used to optimize the percent degradation of methyl orange. The factors investigated were as follows: pH of the solution Eqs 2–8, the initial concentration of methyl orange (50–100 mg/L), the contact time (30–60 min), and the mass of ferromagnetic activated carbon from peanut shells (AC-PS@FeII) (100–200 mg). The optimization of the effects of these factors involved three steps: (i) conducting statistically designed experiments according to the generated experimental plan; (ii) proposing a mathematical model based on the experimental results and the variance analysis; and (iii) predicting the output variable and confirmation of the model. Table 1 presents the levels of the variables involved and the expected response.

TABLE 1 Experimental design parameters.

Influence factor	Coded factor	Coded level		
		−1	0	+1
		Current level		
pH	A	2	5	8
Concentration (mg/L)	B	50	75	100
Mass of AC-PS@FeII (mg) (mg)	C	100	150	200
Contact time (min)	D	30	45	60

The spent catalyst was recovered using an external magnetic field and recycled, washed with distilled water, and reused for three cycles. This reuse of AC-PS@FeII (150 mg) was carried out in a solution at 50 mg/L (MO), pH = 2, H_2O_2 (5 mL), and 60 min of stirring.

For 4 chosen variables and 3 points fixed at the center, the centered composite plan made it possible to carry out 27 experiments determined using Eq. 1.

$$N = 2^K + 2K + KC = 2^4 + (2X4) + 3 = 27, \quad (1)$$

where N is the total number of experiments, K is the number of factors studied, and KC is the number of points at the center, which allows us to determine errors or reproducibility of the data.

The 27 experiments were analyzed using Statgraphics 18.0 software. At the end of this analysis, the optimal values of pH of the solution, initial concentration of the pollutant, contact time, and mass of AC-PS@FeII were obtained, whose values were used for the rest of the work.

The residual concentrations of the dye at different reaction times were determined spectrophotometrically at λ_{max} = 505 nm at an acidic pH range and λ_{max} = 465 nm in basic media. The removal efficiency of methyl orange is defined by Eq. 2:

$$\text{removal efficiency } (\%) = 100\left(1 - \frac{C_t}{C_o}\right), \quad (2)$$

where C_o is the initial concentration of methyl orange and C_t is the concentration of methyl orange at reaction time t (min).

Hydroxyl radicals react with methyl orange to degrade it according to Eq. 3:

$$\text{Methyl orange} + OH\bullet \rightarrow \text{by} - \text{product of compound.} \quad (3)$$

The first-order kinetics is represented by Eq. 4:

$$V = -\frac{d[IC]}{dt} = kC^1. \quad (4)$$

From Eq. 3, we obtain by integration (with $C=C_0$ at $t = 0$)

$$\ln \frac{C}{Co} = kt. \quad (5)$$

The second-order kinetics is represented by Eq. 6:

$$V = -\frac{d^2C}{dt^2} = k.C^2. \quad (6)$$

TABLE 2 Iodine index of different activated carbons.

Activating agent	Impregnation ratio	Agent concentration activator (M)	Iodine index
KOH	1/1	0.5	489
	1/2	1	509
	1/3	1.5	591
H_3PO_4	1/1	0.5	337
	1/2	1	395
	1/3	1.5	328

TABLE 3 Iodine number of activated carbon (AC-PS) and ferromagnetic activated carbon (AC-PS@FeII).

Material	AC-PS	AC-PS@FeII
Iodine value (mg/g)	591	312

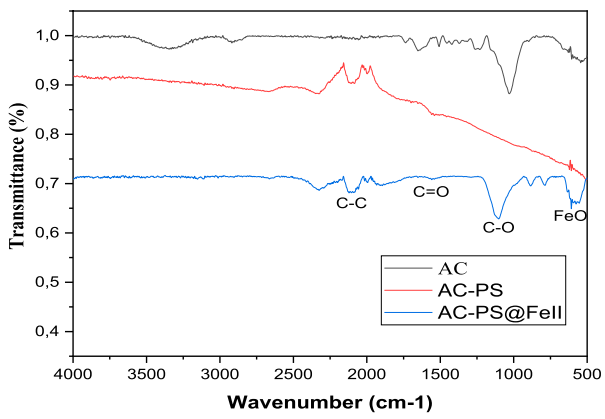

FIGURE 1
Fourier-transform infrared (FTIR) spectrum of materials.

We obtain, by integration (with C=C_0 at t = 0), that for kinetics of order 2,

$$\frac{1}{C_t} - \frac{1}{C_o} = kt, \tag{7}$$

where *Co* is the initial concentration of the pollutant (mg/L); C_t is the concentration of the pollutant at equilibrium (mg/L); and k is the respective rate constant.

3 Results and discussion

3.1 Characterization

3.1.1 Iodine number

The iodine index indicates the degree of activation of activated carbon and is essentially used to measure the micropores (0–20 Å) present on the carbon. To gain an insight into the porosity structure of activated carbons, liquid-phase iodine adsorption has been used extensively in the characterization of activated carbon (Ndi et al., 2014; Sahira and Bhadra, 2014; Tchuifon et al., 2014; Ndifor-Angwafor et al., 2017; Ngakou et al., 2017; Kuete et al., 2018). The iodine index values of the prepared activated carbons are presented in Table 2.

Table 2 shows that, in the case of KOH, the iodine value increases with both concentration and precursor-to-activator solution ratios. For the H_3PO_4 activator, a maximum is reached at 1 M.

These results attest that the type of activating agents used in the preparation of activated carbons, the concentration, and synthesis conditions variously influence the porosity structure of the resulting carbonaceous material. These iodine index characterization tests show higher microporosity in activated carbons prepared from KOH with iodine indexes ranging from 489 to 591 mg/g. This microporosity is very low for carbons prepared from orthophosphoric acid (H_3PO_4) with iodine values between 328 and 395 mg/g. H_3PO_4 retains carbon (promoting the formation of cross-links through dehydration, cyclization, and condensation reactions) and redistributes bio-polymers, which facilitates their conversion to aromatic rings and forms larger pores, consequently reducing iodine adsorption efficiency (Anis et al., 2014). This promotes the formation of a mixture of micropores and large mesopores.

The high iodine values obtained during KOH activation indicate that the KOH oxygen eliminated cross-linking and stabilized the carbon atoms in the crystallites. During pyrolysis, the intercalation of K atoms, resulting from the reduction of potassium hydroxide, is the initial step in the degradation process of biomass activated with KOH. This intercalation of potassium metal forces the lamellae apart in the crystal. This spacing in the crystal promotes the development of the carbonaceous structure and the porous network (Sahira and Bhadra, 2014). In other words, the development of this porosity in KOH-activated carbons is associated with a gasification reaction as KOH is reduced to potassium metal during the carbonization process. The reaction of KOH and carbon is postulated to occur according to Eq. 8 (Li et al., 2004):

$$6KOH + 2C \rightarrow 2K + 3H_2 + 2K_2CO_3. \tag{8}$$

In general, higher iodine values denote greater adsorption capacity. Thus, the iodine values (Table 2) show that KOH is a better activating agent than H_3PO_4 for the preparation of carbons from peanut shells. However, the iodine values reported vary from the values reported in the literature for activated carbons activated with potassium hydroxide (Okieimen et al., 2007; Sahira

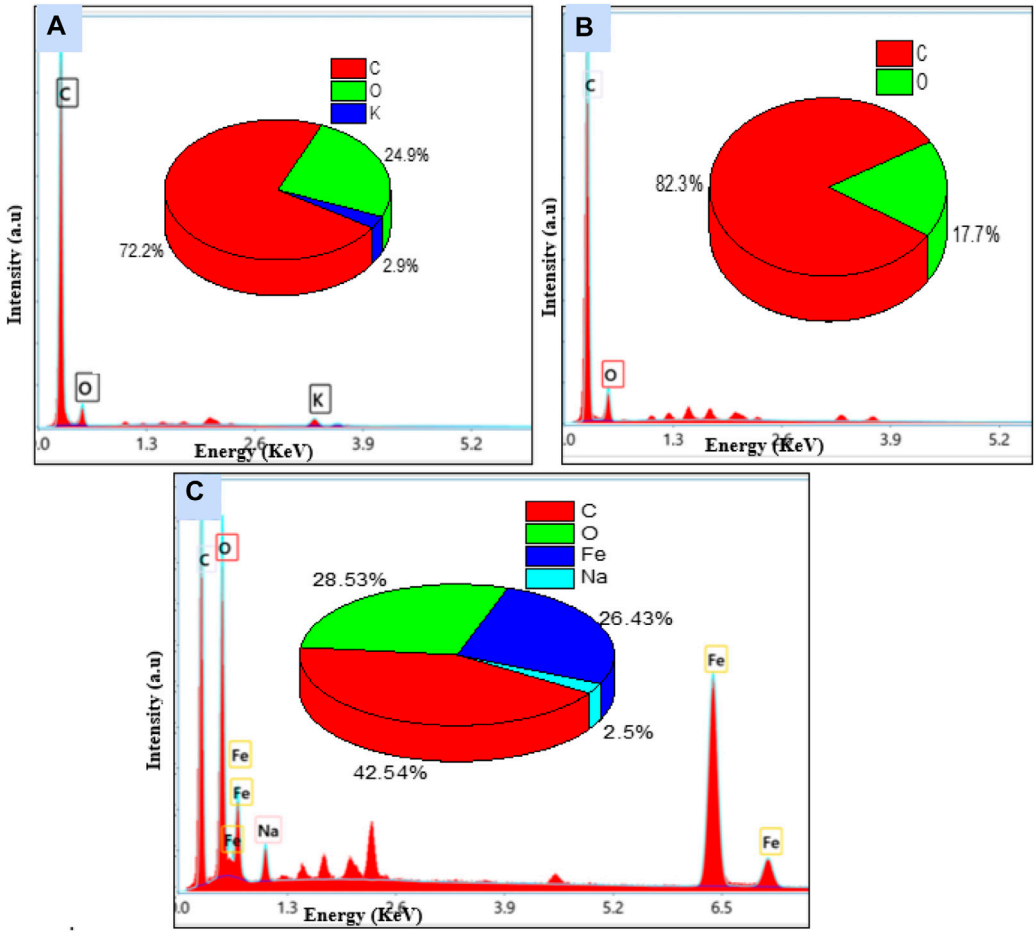

FIGURE 2
Energy-dispersive X-ray images of **(A)** peanut shells **(B)** activated carbon **(C)** ferromagnetic activated carbon.

and Bhadra, 2014; Kuete et al., 2018). This is due to differences in the composition of the precursor material and synthesis conditions.

In the remainder of this work, the activated carbon with the greatest iodine index value was used and coded as AC-PS, whereas the iron oxide-modified activated carbon was coded as AC-PS@FeII. The iodine index of PS@FeII was determined, and relative performance with pristine carbon is presented in Table 3.

Based on the iodine index values given in Table 3, the pristine activated carbon (AC-PS) is more porous than the functionalized activated carbon (AC-PS@FeII) consistent with the pore volumes reported in nitrogen adsorption–desorption studies. This is due to the occupation of the pores of the activated carbon by iron oxides during treatment.

3.1.2 Fourier-transform infrared spectroscopy

FTIR spectroscopy was used to identify different surface functional groups, the pristine carbon, KOH-activated carbons, and ferromagnetic carbons (AC, AC-PS, and AC-PS@FeII), over a wavelength range of 500–4,000 cm^{-1}. The infrared spectra of the materials are shown in Figure 1.

The FTIR spectra of the three materials, namely, AC, AC-PS, and AC-PS@FeII, show that in the region between 2,500 and 2,000 cm^{-1}, characteristic peaks of C–C aliphatic stretching vibrations appear. The peaks appearing at 1,600 cm^{-1} on these spectra are attributed to the stretching of the C=O carbonyl groups of the ketones, aldehydes, and/or lactones. The bands around 1,583 cm^{-1} attributed to the elongation vibrations of C=O groups remained unchanged and have almost the same intensities on the dried peanut shells as on the activated, calcined, and magnetized peel. The slight decrease in the intensity of the peaks was observed following pyrolysis. The peaks centered at 1,100 cm^{-1} for ferromagnetic activated carbon AC-PS@FeII and 1,050 cm^{-1} are attributed to the stretching vibrations of ether C–O (Lall et al., 2020; Djouonkep et al., 2022). The appearance of two new bands on the AC-PS@FeII spectra around 750 and 1,000 cm^{-1} is the characteristic of the OH in- and out-of-the-plane bending vibrations of the Fe–OH group in goethite, respectively (Khelifi et al., 2016). Additional differences between the three FTIR spectra were noted. For the spectrum of AC-PS@FeII, a band is observed at 560 cm^{-1} corresponding to iron oxides (FeO). The band between 450 and 740 cm^{-1} was attributed to the Fe–O vibrations of iron oxide nano AC-PS particles (Ngankam et al., 2020). This denotes the successful precipitation of iron oxide after the functionalization of AC-PS to obtain ferromagnetic activated carbon, AC-PS@FeII.

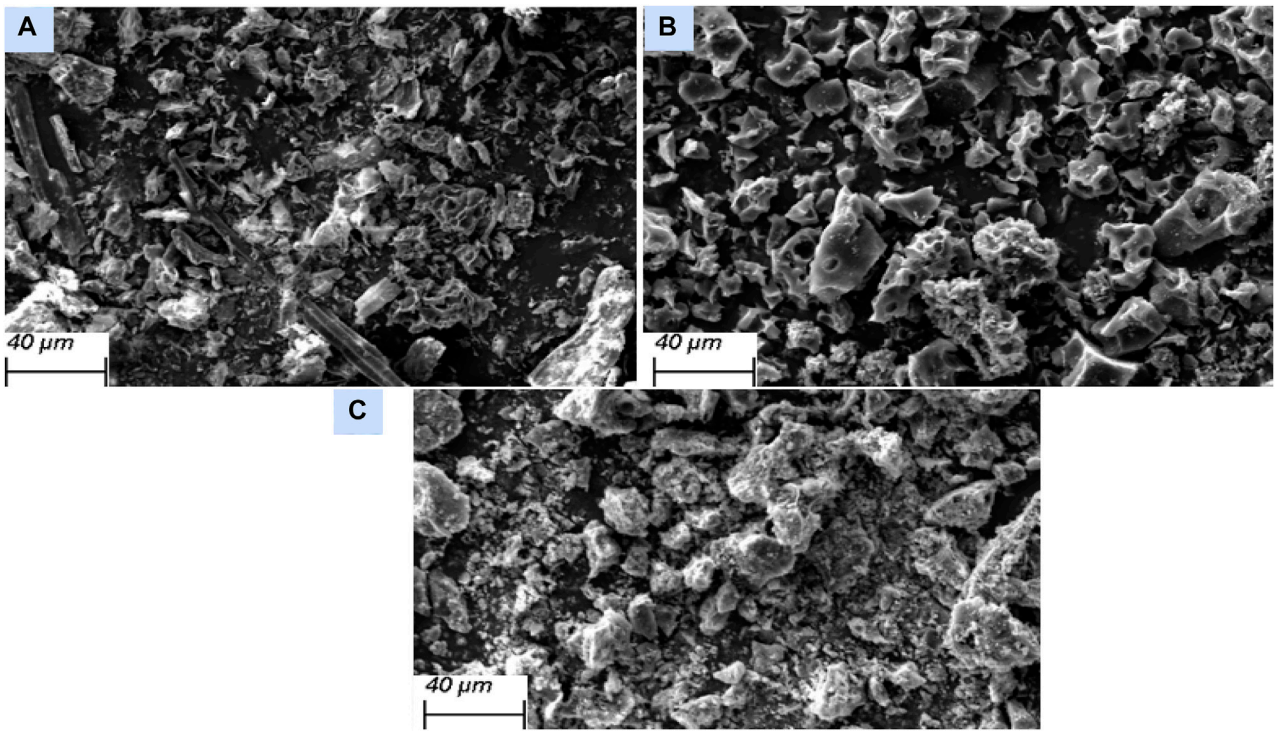

FIGURE 3
Scanning electron microscopy (SEM) images of **(A)** precursor peanut shells **(B)** AC-PS, and **(C)** AC-PS@FeII.

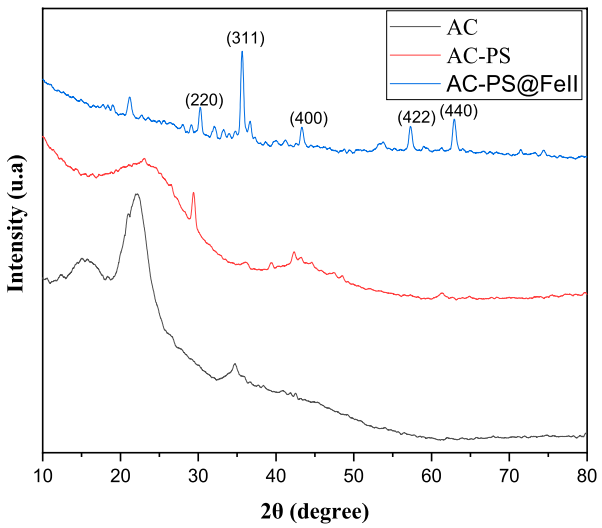

FIGURE 4
X-ray diffractogram.

3.1.3 EDX and SEM of AC-PS and AC-PS@FeII

Energy dispersive X-ray spectroscopy (Figure 2) was used to inspect the elemental composition of the materials. The pie charts presented in each of these figures provide the percentages of the main chemical elements present in the structure of each of these three materials. The chemical composition includes the raw materials, i.e., carbon (72.2%), oxygen (24.9%), and potassium (2.9%), and activated carbon, i.e., carbon (82.3%) and oxygen (17.7%), while ferromagnetic activated carbon contains carbon (42%), oxygen (24%), sodium (8%), and iron (26%) (Figure 2C). EDX analysis revealed the presence of the elements Fe, O, and C on the surface of the ferromagnetic activated carbon, consistent with the formation of iron oxides observed from the FTIR spectrum. The disappearance of elements (K) could be due to dissolution into the aqueous phase and the appearance of the new elements (Fe and Na) arising from the elemental composition of the synthesis materials.

Figure 3A shows the SEM image of the precursor peanut shells. The biomass has a surface morphology in the form of heterogeneous cavities with irregularly agglomerated dispersed clumps of particles. The SEM image of the activated carbon (Figure 3B) shows a sponge-like structure with enhanced porosity as a result of the chemical activation process. The SEM image of the ferromagnetic activated carbon (Figure 3C) shows a surface covered with dispersed particles of iron oxides that clog the pores (Aurelien et al., 2022; Peng et al., 2022).

3.1.4 XRD analysis

XRD was used to determine the crystallinity of the raw material compared to the activated carbon and mineral phases of iron in the ferromagnetic activated carbon. The diffractograms are given in Figure 4.

For the raw material, the peak observed at $2\theta = 23^{\circ}$ is attributed to different planar crystal structures of carbon (Dong et al., 2020). In terms of crystallinity, much of the structure of the activated carbon is amorphous based on the diffractogram pattern. The peaks around

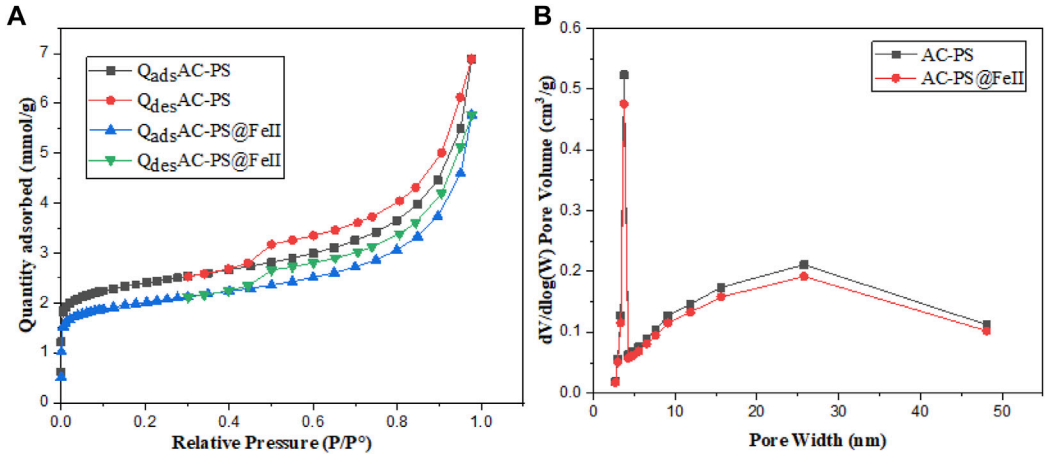

FIGURE 5
Nitrogen adsorption hysteresis **(A)** and BJH pore-size distribution of carbons **(B)** AC-PS and AC-PS@FeII.

TABLE 4 BET specific surface area, total volume, and average pore diameter.

Sample	BET surface ($m^2.g^{-1}$)	Total pore volume ($cm^3.g^{-1}$)	External surface area ($m^2.g^{-1}$)	Micropore area ($m^2.g^{-1}$)	Micropore volume ($cm^3.g^{-1}$)
AC-PS	199.6915	0.281291	92.3059	107.3856	0.059523
AC-PS@FeII	181.9629	0.161121	82.7487	99.2142	0.054835

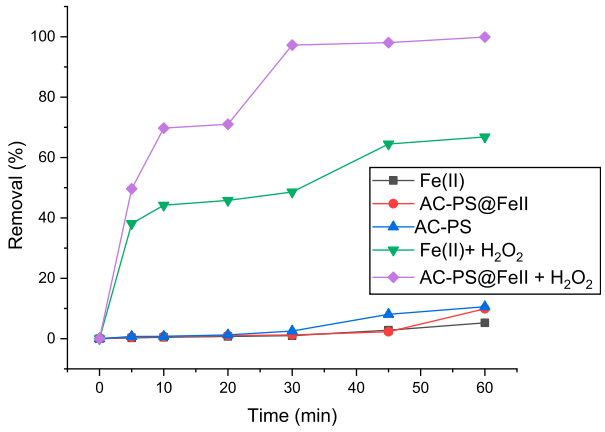

FIGURE 6
Degradation of methyl orange (MO) under different conditions at pH 2, 50 mg/L OM, and 150 g of AC-PS@FeII.

2θ = 30° and 2θ = 44° were attributed to the planar crystal structure of the activated carbon (Sandrale et al., 2023). The diffractogram of AC-PS@FeII portrayed at least five well-pronounced peaks, indicating the existence of different crystalline phases. The peaks at 2θ values of 30°, 35°, 44°, 55°, and 65° of AC-PS@FeII are the characteristic of magnetite (Fe_3O_4), which indicates a cubic spinel structure of indexed peaks like (220), (311), (400), (422), and (400) (Dong et al., 2020). The presence of crystalline phases of iron confirms the insertion of iron ions into the carbon. These crystalline phases essentially consist of magnetite (Fe_3O_4) and maghemite (γ-Fe_2O_3) at 2θ = 35°. Only magnetite (Fe_3O_4) has a ferromagnetic character, and the other phase is paramagnetic.

3.1.5 BET-specific surface area and porosity

The results of the nitrogen adsorption hysteresis at 77 K by different carbons are given in Figure 5A, and the pore-size distribution of the carbons is given in Figure 5B.

Figure 5A shows the N_2 adsorption–desorption isotherms and pore-size distribution obtained for the AC-PS and AC-PS@FeII samples. Although the isotherms present a combined type I/II characteristic (IUPAC, 1985), the type I isotherm characterized for microporous solids occupies a major part. The pore parameters given in Table 4 indicate that the formation of iron oxide nanoparticles inside the porous structure of the activated carbon causes a reduction in the BET surface area and pore volume (Zhang et al., 2007). The BET surface area and pore volume values are given in Table 2. The analysis of the pore size by the BJH method (Figure 5B) highlights the microporous nature of the activated carbon and AC-PS@FeII. Similar results were obtained by Kpinsoton (2019) on the development of catalysts based on activated carbon and laterites for the degradation of methylene blue by the heterogeneous Fenton process.

The catalyst thus prepared was used to degrade methyl orange dye by optimizing the percent degradation using the response surface methodology.

TABLE 5 Experimental design matrix and predicted values for the degradation of methyl orange in the presence of AC-PS@FeII

N°	A: pH	B: *adsorbate concentration* (mg/L)	C: catalyst dose (mg)	D: time (min)	Degradation efficiency (%)	
					Observed value	Predicted value
1	2	50	100	30	83.1096	83.0243
2	8	50	100	30	9.4742	7.82268
3	2	100	100	30	67.4309	74.6614
4	8	100	100	30	4.38548	5.79258
5	2	50	200	30	88.0515	89.7459
6	8	50	200	30	5.25818	12.6544
7	2	100	200	30	69.8893	70.4125
8	8	100	200	30	7.13681	−0.346257
9	2	50	100	60	71.9965	81.6749
10	8	50	100	60	11.8144	10.6065
11	2	100	100	60	79.0708	70.9898
12	8	100	100	60	5.75319	6.25412
13	2	50	200	60	99.4907	97.3988
14	8	50	200	60	29.4755	24.4404
15	2	100	200	60	71.8962	75.7431
16	8	100	200	60	9.71701	9.11751
17	2	75	150	45	96.5557	83.8405
18	8	75	150	45	6.25407	12.9269
19	5	50	150	45	43.3261	34.6288
20	5	100	150	45	20.1308	22.7858
21	5	75	100	45	28.7715	20.9803
22	5	75	200	45	24.024	25.7729
23	5	75	150	30	27.2381	18.2066
24	5	75	150	60	19.2746	22.2638
25	5	75	150	45	18.8246	25.2344
26	5	75	150	45	19.3759	25.2344
27	5	75	150	45	19.3759	25.2344

3.2 Catalytic degradation

The degradation of MO was studied by different processes, i.e., the homogeneous Fenton process (Fe(II) + H_2O_2), adsorption onto AC-PS, Fe(II), and AC-PS@FeII, and finally, heterogeneous Fenton (AC-PS@FeII + H_2O_2) in a solution of 50 mg/L (MO) at pH 2 with 60 min of stirring and 0.5 mL of H_2O_2, and the results are given in Figure 6.

The results (Figure 6) indicate neither degradation effects nor adsorption when Fe(II) alone is used, a low removal efficiency of 5% for AC-PS@FeII, and a significantly higher removal efficiency of 16.60% for AC-PS alone. This low adsorption (~5%) could be due to the occupation of the AC-PS cavities and obstruction of the active adsorption sites by magnetite particles, resulting in the low affinity of AC-PS@FeII for the MO molecules. When the mineralization potential of Fe(II) + H_2O_2 was examined, a removal efficiency of 66.81% was observed under similar conditions. This removal is due to the generation of hydroxide radicals, which leads to the oxidation of MO. Maximum removal is achieved at 99.86% (50 mg/L of MO) for the heterogeneous Fenton process using AC-PS@FeII + H_2O_2 as a catalyst. It is demonstrated that MO sequestration efficiency using heterogeneous Fenton catalysis exceeds the use of the other approaches.

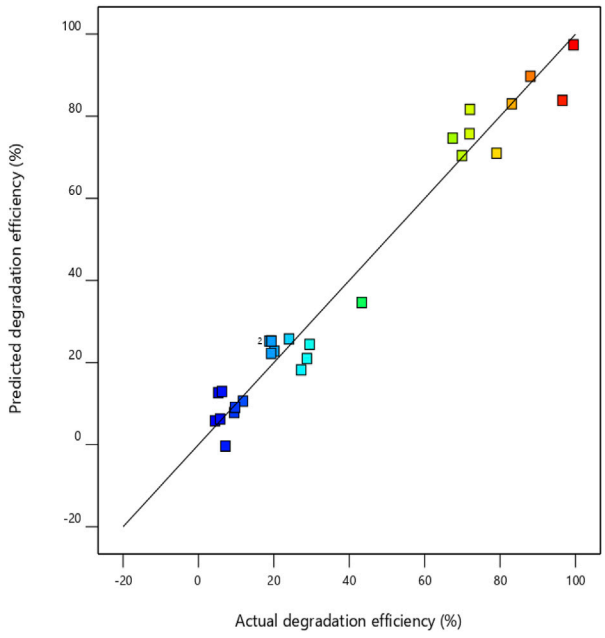

FIGURE 7
Comparison of predicted and actual values for the degradation efficiency (%) of methyl orange.

3.3 Degradation of methyl orange by the heterogeneous Fenton process

The efficiency of AC-PS@FeII to degrade MO was optimized using the response surface methodology using solution pH (A), MO concentration (B), catalyst dosage (C), and contact time (D) as the input variables, and the results are hereby presented.

3.3.1 Optimization of the removal of methyl orange

AC-PS@FeII was used in the optimization studies based on the central composite experimental design of the response surface methodology since it exhibited the highest catalytic activity. Table 5 displays the design matrix with 27 runs conducted in a single block, together with the experimental and predicted responses. For each of the 27 experimental runs, the residue values are much smaller than the experimental and theoretical values, indicating that the experimental and theoretical values are reasonably approximated. This is supported by the near-unity R^2 (96.60%) and R^2_{adj} (92.64%) values.

The quadratic mathematical model suitably represented the correlation between predicted values (Eq. 9) and the experimental values (Eq. 10).

3.3.1.1 Model with coded values of variables of the design of experiments

$$\begin{aligned}\text{Degradation efficiency}_{coded} = {} & 42.33 - 35.46A - 5.92B + 2.4C \\ & +2.03D + 1.58AB - 0.4725AC \\ & +1.03AD - 2.74BC - 0.5806BD \\ & +2.25CD + 23.15A^2 + 3.47B^2 \\ & -1.86C^2 - 5.00D^2.\end{aligned} \quad (9)$$

3.3.1.2 Model with actual values of variables of the design of experiments

$$\begin{aligned}\text{Degradation efficiency}_{Actual} = {} & 123.731 - 39.6844A - 0.77711B \\ & +0.316139C + 1.68612D \\ & +2.57214A^2 + 0.0211094A*B \\ & -0.00314986A*C + 0.0229618A*D \\ & +0.00555659B^2 - 0.00219411B*C \\ & -0.00154815C*B - 0.00154815B*D \\ & -0.000743133C^2 \\ & +0.00300074*C*D - 0.0222188D^2.\end{aligned} \quad (10)$$

These equations have terms with negative and positive coefficients. A positive coefficient indicates that the factor or interaction concerned has a synergistic effect on the response. When one of such parameters is increased, an increase in the degradation rate, and otherwise, a decrease in the degradation rate is observed. Contrarily, a negative coefficient indicates that the factor has an antagonistic effect on the degradation rate. Its increase leads to a reduction in the rate of degradation and a reduction in the factor that favors it (Kouotou et al., 2021).

It follows that pH, concentration, pH–mass interaction, concentration–mass, concentration–time, mass–mass, and time–time have antagonistic effects, while mass, time, pH–pH interaction, pH–time, concentration–concentration, and mass–time have synergistic effects on the degradation rate.

Of all these interactions, the significant interactions could be determined by the analysis of variance (ANOVA). The probability plot (Figure 7) illustrates a close relationship between the responses predicted by the model and those found empirically, in addition to the values of R^2 and R^2adj that demonstrate the validity of this model. These results are confirmed by the relationship between the

TABLE 6 Predicted and experimental values for the degradation efficiency of methyl orange under the optimal condition.

Condition				Degradation efficiency (%)		
pH	Adsorbate concentration (mg/L)	Adsorbent dose (mg)	Time (min)	Predicted value	Experimental value	Error percentage
2	50	200	50	99.22	99.49	0.27

TABLE 7 Analysis of variance for the quadratic model of the degradation efficiency of methyl orange.

Source	Sum of squares	df	Mean square	F-value	*p*-value	Remark
Model	26,420.87	14	1,887.20	24.37	< **0.0001**	**Significant**
A-pH	22,629.32	1	22,629.32	292.21	< **0.0001**	**significant**
B-adsorbate concentration	631.15	1	631.15	8.15	**0.0145**	**significant**
C-adsorbent dose	103.36	1	103.36	1.33	0.2705	
D-time	74.07	1	74.07	0.9565	0.3474	
AB	40.10	1	40.10	0.5179	0.4855	
AC	3.57	1	3.57	0.0461	0.8336	
AD	17.08	1	17.08	0.2206	0.6470	
BC	120.35	1	120.35	1.55	0.2363	
BD	5.39	1	5.39	0.0696	0.7963	
CD	81.04	1	81.04	1.05	0.3265	
A^2	1,378.00	1	1,378.00	17.79	**0.0012**	**significant**
B^2	31.01	1	31.01	0.4005	0.5387	
C^2	8.88	1	8.88	0.1146	0.7408	
D^2	64.27	1	64.27	0.8299	0.3802	
Residual	929.30	12	77.44			
Lack of fit	929.10	10	92.91	917.08	0.0011	
Pure Error	0.2026	2	0.1013			
Cor total	27,350.17	26				

experimental and predicted values R^2 (96.60%) and R^2adj (92.63%), showing good proximity between the values predicted by the model and those obtained experimentally. Table 6 lists the best process conditions for the highest response (degradation efficiency) with the associated error value.

3.3.2 ANOVA

ANOVA makes it possible to evaluate the influence, if any, of different factors and their interactions and verify the validity of the mathematical model. The ANOVA data of the model are given in Table 7:

For this analysis, the probability p was used to evaluate the significant effects of the factors and their interaction, and the indicator of the fineness of the second-order polynomial model obtained is the value of the coefficient of determination, R^2. A factor or an interaction between factors is said to be significant when the probability p is less than 0.005 ($p < 5\%$). In addition, the value of the coefficient of determination must be close to 1 (Kimouche, 2008). The results are given in Table 7. The degradation efficiency was significantly ($p < 0.05$) affected by the solution pH and the initial concentration of the dye. The solution pH alters the surface chemistry of the catalyst and, hence, the activity of the catalytically active sites. The initial concentration controls the mass gradient of the dye across the boundary layer to the catalyst surface and the radicals and accessibility to the limited catalyst. Beyond 50 mg/L, the dye concentration exceeds the available radicals, leading to decreased degradation efficiency. Uncharacteristically, the catalyst dosage had no statistically significant effect on the degradation efficiency. This suggests that the increase in the adsorbent dosage resulted in the degradation of the finite amount of H_2O_2 to O_2 and the concomitant quenching of OH^* radicals by Fe^{2+} ions in the solution (Dat et al., 2023).

3.3.3 Response surfaces

Figure 8 shows in 3D the effect of two variables on the degradation efficiency when the other variables are fixed at zero. A relative significant interaction was observed between the initial dye concentration and pH. A decrease in dye concentration and an increase in pH favored the degradation efficiency. In the literature, the removal efficiency of dyes using the heterogeneous Fenton process is dependent on pH. A pH range of 2–3 is often optimal for Fenton degradation because complexes and insoluble ferric hydroxide form in the solution at pH values above 3, and the quantity of $OH^{\bullet}$ radicals needed for the oxidation of the dye is significantly reduced, which explains the notable decrease in the percentage degradation obtained with higher pH values (Hassan and Hameed, 2011; Muhammad and Mashi, 2020; Ngankam et al., 2020). Fewer investigations, however, demonstrate that high yields of degradation at pH levels (in an acidic medium with pH 2 and 4) result from the impregnation of magnetic particles in the form of iron oxides (Figure 8). The optimum process conditions were identified from the 3D model plots. The optimal degradation

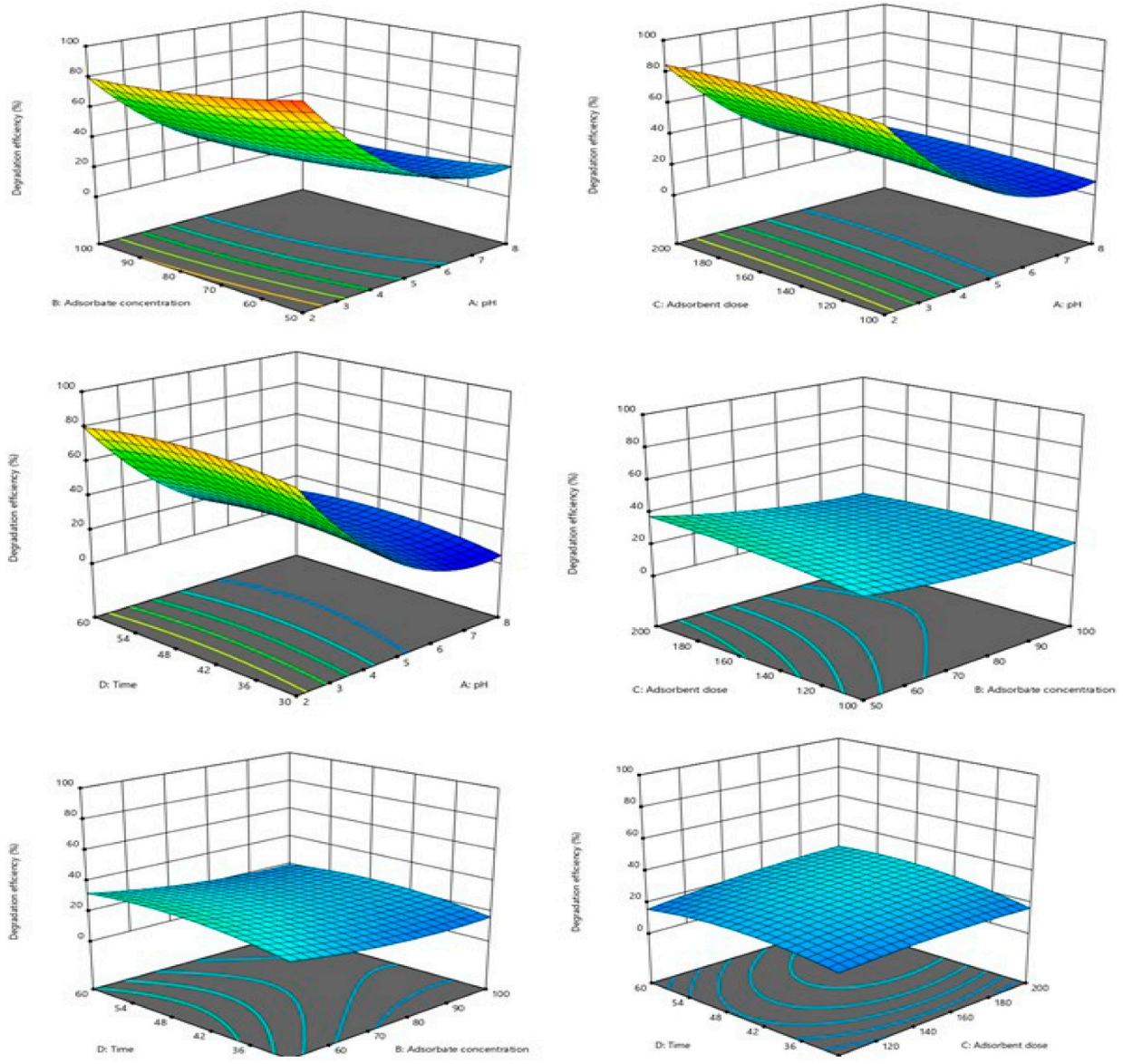

FIGURE 8
Effects of pH, adsorbate concentration (mg/L), adsorbent dose (mg), and time (min), and their interactions on the removal efficiency (%) of methyl orange.

conditions were as follows: 0.2 g/50 mL of AC-PS@FeII, the concentration of the pollutant at 50 mg/L, and pH = 2 at a contact time of 50 min for a degradation rate of 99.22%.

3.4 Kinetic studies of degradation

3.4.1 First- and second-order kinetics of methyl orange degradation

Determining the kinetics of organic pollutant degradation and H_2O_2 decomposition is a challenging task since numerous mechanisms can alter the apparent rate of the Fenton reaction (Bopda et al., 2022). To simplify, the Fenton process degradation reaction of an organic chemical can be characterized by a pseudo first-order kinetic rule (Eq. 10a) that assumes a quasi-stationary concentration of hydroxyl radicals created in the medium.

$$\frac{dC}{dt} = -kC \rightarrow \ln \frac{C_0}{C_t} = kt. \tag{10a}$$

The second-order kinetic model (Eq. 11) was also used to describe the degradation of an organic dye by the Fenton process (Kenda et al., 2023):

$$\frac{dC}{dt} = -kC^2 \rightarrow \frac{1}{C_t} - \frac{1}{C_0} = kt. \tag{11}$$

The linear regression of the experimental points can be used to determine the kinetic rate constant by tracking the pollutant

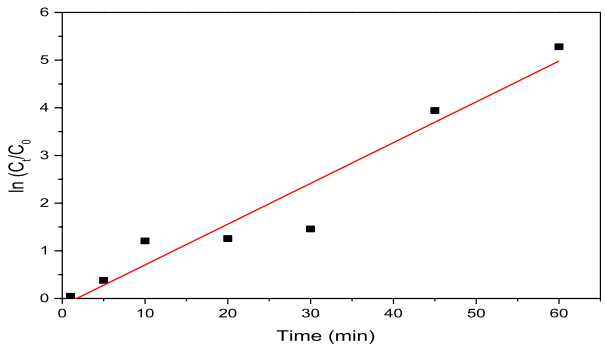

FIGURE 9
Pseudo first-order kinetic model applied to the degradation of methyl orange on ferromagnetic activated carbon.

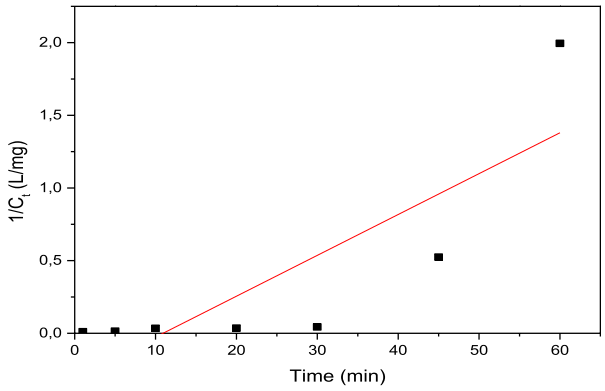

FIGURE 10
Pseudo second-order kinetic model applied to the degradation of methyl orange on the ferromagnetic activated carbon.

TABLE 8 Kinetic parameters of methyl orange degradation.

Pseudo first-order		Pseudo second-order			
K (min^{-1})	$t_{1/2}$ (min)	R^2	K_2 (min^{-1})	$t_{1/2}$ (min)	R^2
0.0855	8.07	0.9361	0.0281	24.55	0.699

degradation over time. Only at the beginning of the reaction, before the substantial intermediates have formed, can the kinetic parameters be determined (Mafo et al., 2023):

The pseudo first- and pseudo second-order kinetics were studied, and the results are presented in Figures 9, 10, respectively. Table 8 presents the first- and second-order kinetic parameters. Figure 9 presents the pseudo first-order kinetic model applied to the degradation of methyl orange on ferromagnetic activated carbon.

As shown in Table 8, the pseudo first-order model best described the degradation kinetics of the methyl orange dye since the coefficient of determination was closest to unity (R^2 = 0.936).

3.5 Comparison with other catalysts

Table 9 presents data from the literature on the elimination of some dyes by different heterogeneous Fenton catalysts for comparison with those obtained with AC-PS@FeII. This experiment made it possible to have optimal degradation conditions, such as 200 mg of ferromagnetic activated carbon, the concentration of the pollutant at 50 mg/L, and pH = 2 at a contact time of 50 min for a degradation rate of 99.22%.

3.6 Characterization of the material after degradation

After degradation, the exhausted material was analyzed to evaluate any chemical changes. Figure 11A shows the results of the EDX analysis. These two figures show that the percentages of the elements are not identical. The change in the carbon percentage is from 42.54% to 49.85. The decrease in the percentage of iron is attributed to the reaction between iron and H_2O_2 for the production of hydroxyl radicals in the medium for the elimination of methyl orange in an aqueous medium. The SEM analysis (Figures 11A, B) shows that the two materials AC-PS@FeII-A and AC-PS@FeII-B have the same surfaces. This shows that the use of the CA-FeII material for water treatment does not affect surfaces too much, although the percentages of the elements are slightly modified.

3.7 Stability and reusability of the catalyst

The stability and reusability of the material are important factors in catalysis. The degradation of methyl orange was repeated four times using the same catalyst. The spent catalyst was recoverable using a simple magnet. The same degradation of methyl orange is observed without the loss of catalytic activity during the first two cycles and a slight loss of activity during the third and fourth cycles (Figure 12). The stability and efficiency of the material (AC-PS@FeII) were substantially lost after the third cycle. This is attributed to the decrease in the reactive iron content.

3.8 Mechanism of degradation of methyl orange

The reaction pathway (Figure 13) shows the proposed reaction mechanism for the Fenton process elimination of methyl orange from the aqueous solution:

Figure 13 shows the degradation pathway of methyl orange by the Fenton process, showing the formation of intermediates during the degradation process. The process included the following steps: step 1 shows that methyl orange degradation occurs through the cleavage of the azo group connecting two aromatic rings. The azo group—N=N—can convert to amines when adsorbed on the iron surface; step 2 shows two compounds that can correspond to benzenesulfonic acid and aniline; step 3 corresponds to the

TABLE 9 Comparative results of dyes removed by various heterogeneous Fenton processes based on different media in recent years.

Material	Dye	Optimum dosage reaction condition	Observation	Reference
Fe@ACFs	Reactive red M-3BE 50 μM	5 g/L Fe@ACFs, 30 mM of H_2O_2, pH = 2.95, T = 50°C	99.8% elimination in 30 min	Yao et al. (2013)
Catalyst Fe/Ca	Orange II 0.1 mM	0.1 g. L^{-1} of Fe/Ca and 6 mM of H_2O_2, T = 30°C, and pH 3	95% of degradation and 60% elimination of TOC in 5 h	Duarte et al. (2013)
Catalyst Fe/Ca	Orange II 0.1 mM	0.1 g·L^{-1} of Fe/Ca, T = 30°C, pH = 3	90% of decoloration in 4 h and 61% elimination of TOC in 24 h	Duarte et al. (2013)
Fe–montmorillonite K10	Acide Red 1 50 mg·L^{-1}	5 g/L of Fe–MK10 and 16 mM of H_2O_2, pH = 2.5	99% of decoloration in 2 h 30 min	Daud et al. (2010)
Fe3–xTixO4	Methylene blue 100 mg. L^{-1}	3.0 g·L^{-1} of $Fe_{2\text{-}22}Ti0._{78}O_4$ et 0.30 mol. L^{-1} of H_2O_2, pH 6.8	95% of degradation in 7 h	Yang et al. (2009)
Catalyst Fe/Ca	Orange II 0.1 mM	Ccat. = 0.2 g/L and 6 mM of H_2O_2, T = 30.8°C, and pH 3.0	>95% of degradation in 3 h	Ramirez et al. (2007)
CA-FeOx 400/400	Methylene blue 10 mg·L^{-1}	5 g/L Ca-FeOx and 30 mM of H_2O_2 at pH = 3.25	>95% of degradation in 6 h	Gloria (2010)
Catalyst CA-HP@FeII	Brilliant blue 50 mg·L^{-1}	0.33 g/L CA-HP@FeII, pH 2	96% in degradation in 3 h	Mazilu et al. (2017)
Catalyst AC-PS@FeII	Methyl orange 50 mg·L^{-1}	0.2 g/L AC-PS@FeII, pH 2	99% of degradation in 50 min	Present work

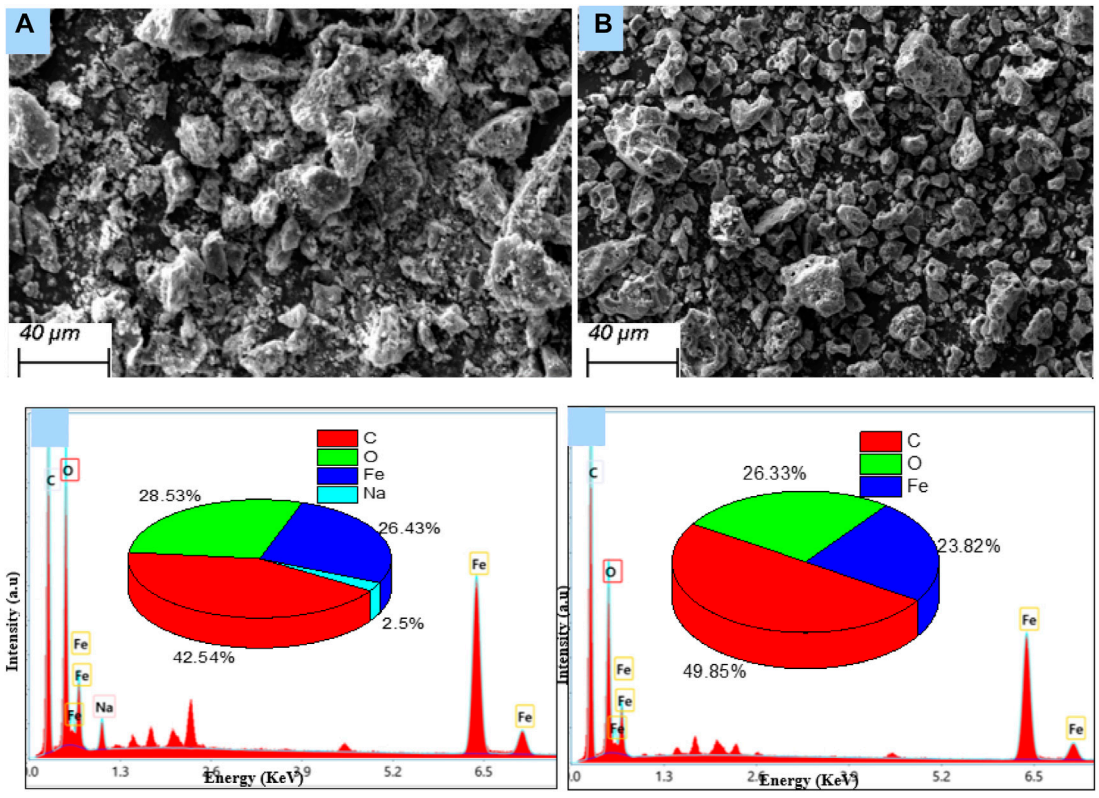

FIGURE 11
SEM and EDX images of AC-PS@FeII (A) before and (B) after methyl orange degradation.

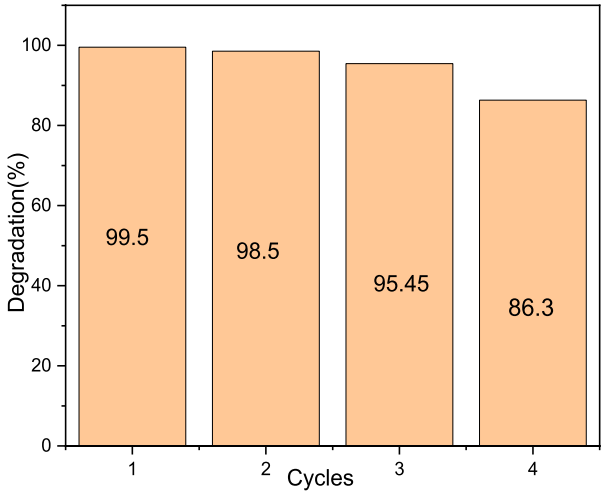

FIGURE 12
Four cycles of MO degradation by AC-PS@FeII

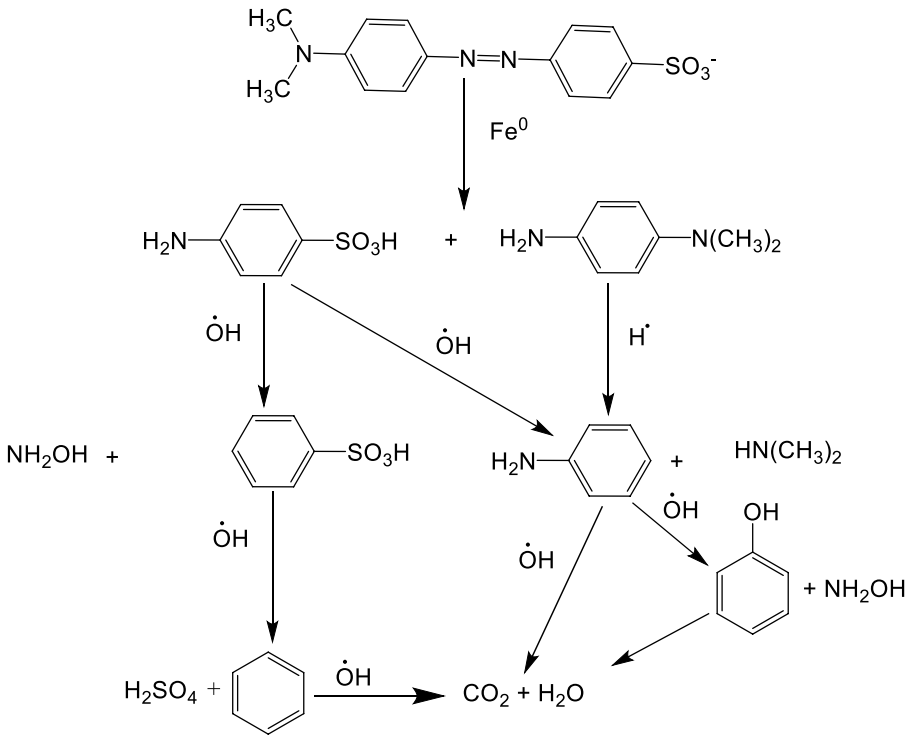

FIGURE 13
Degradation mechanism of methyl orange.

formation of benzene and phenol. This shows that benzene can be a stable intermediate during the reaction; and step 4 shows the formation of CO_2 and H_2O, confirming the complete degradation of the dye. The mechanism is consistent with that described by Gomathi Devi et al. (2008). However, in the absence of mass spectrometry data for the identification of intermediates, the mechanism could not be validated.

4 Conclusion

The objective of the present work was to prepare a ferromagnetic activated carbon from PSs for the Fenton-type degradation of MO with optimized textural properties and corresponding synthesis conditions. Based on the iodine indexes, KOH-activated carbon adsorbents exhibited higher porosity than the H_3PO_4-activated

counterparts. The physicochemical characterizations of the pristine activated carbon (AC-PS) and the ferromagnetic activated carbon (AC-PS@FeII) showed a decrease in the surface area and pore volume due to the precipitation of magnetite particles. Heterogeneous Fenton catalytic degradation of MO using AC-PS@FeII exhibited higher degradation capability than adsorption using AC-PS and iron nanoparticles. The influence of parameters such as catalyst mass, pH, contact time, and pollutant concentration was studied, and the degradation experiment was optimized using RSM design. The optimal degradation conditions were as follows: 0.2 g/50 mL of AC-PS@FeII, the concentration of the pollutant at 50 mg/L, and pH = 2 at a contact time of 50 min for a degradation rate of 99.22%. The results of recyclability revealed a slight decrease in degradation capacity after four cycles, which showed that AC-PS@FeII is a potential candidate as a hetero-Fenton catalyst for water treatment.

Data availability statement

The original contributions presented in the study are included in the article/Supplementary Material; further inquiries can be directed to the corresponding author.

Author contributions

JN: project administration, resources, and writing–review and editing. JM: formal analysis, methodology, software, validation, visualization, and writing–review and editing. DT: data curation, formal analysis, software, visualization, and writing–review and editing. SM: visualization, software, and writing–original draft. CF: conceptualization, methodology, validation, visualization, and writing–review and editing. MC: data curation, formal analysis, software, and writing–review and editing. PT: conceptualization, supervision, validation, visualization, writing–original draft, and writing–review and editing.

Funding

The author(s) declare that no financial support was received for the research, authorship, and/or publication of this article.

Conflict of interest

The authors declare that the research was conducted in the absence of any commercial or financial relationships that could be construed as a potential conflict of interest.

Publisher's note

All claims expressed in this article are solely those of the authors and do not necessarily represent those of their affiliated organizations, or those of the publisher, the editors, and the reviewers. Any product that may be evaluated in this article, or claim that may be made by its manufacturer, is not guaranteed or endorsed by the publisher.

References

Anis, D., Ishak, M. A. M., Khudzir, A. G. Z. I., Iqbaldin, M. N., Uwaisulqarni, M. O., and Nawawi, W. I. (2014). *Production of rubber seed pericarp based activated carbon using microwave-induced different chemical activating agent* 4 (7), 1–8.

Aurelien, B., Sandrale, G., Josiane, N. N., Georges, T. K., Cyrille, G. F., Tiotsop Kuete, I.-H., et al. (2022). Ferromagnetic biochar prepared from hydrothermally modified calcined mango seeds for fenton-like degradation of indigo carmine , 8, 81. doi:10.3390/c8040081

Bernardi, F., Fecher, G., Alves, M., and Morais, J. (2010). Unraveling the formation of Core–Shell structures in nanoparticles by S-xps. *J. Phys. Chem. Lett.* 1, 912–917. doi:10.1021/jz100049Z

Bopda, A., Mafo, S. G. M., Josiane N, N., Kenda, G. T., Fotsop, C. G., Kuete, I. H. T., et al. (2022). Ferromagnetic biochar prepared from hydrothermally modified calcined mango seeds for fenton-like degradation of indigo carmine. *J. Carbon Res.* 8, 81. doi:10.3390/c8040081

Chimi, T., Hannah, U., Nintedem, M. L., Mboumbouo, B. J., Tome, S., Hermann, D. T., et al. (2022). Preparation, characterization and application of H3PO4-activated carbon from Pentaclethra macrophylla pods for the removal of Cr(VI) in aqueous medium. *J. Iran. Chem. Soc.* doi:10.1007/s13738-022-02675-9

Cleveland, V., Bingham, J. P., and Kan, E. (2014). Heterogeneous Fenton degradation of bisphenol A by carbon nanotube-supported Fe3O4. *Sep. Purif. Technol.* 133, 388–395. doi:10.1016/j.seppur.2014.06.061

Couture, R., Rose, J., Kumar, N., Mitchell, K., Wallschläger, D., and Cappellen, P. (2013). Sorption of arsenite, arsenate, and thioarsenates to iron oxides and iron sulfides: a kinetic and spectroscopic investigation. *Environ. Sci. Technol.* 47, 5652–5659. doi:10.1021/es3049724

Cuerda-Correa, E. M., Alexandre-Franco, M. F., and Fernández-González, C. (2020). Advanced oxidation processes for the removal of antibiotics from water. An overview. *Overv. Water* 12, 102. doi:10.3390/w12010102

Dat, N. D., Huynh, Q. S., Tran, K. A. T., and Nguyen, M. L. (2023). Performance of heterogeneous Fenton catalyst from solid wastes for removal of emerging contaminant in water: a potential approach to circular economy. *Results Eng.* 18, 101086. doi:10.1016/j.rineng.2023.101086

Daud, N. K., Ahmad, M. A., and Hameed, B. H. (2010). Decolorization of acid red 1 dye solution by fenton-like process using Fe–montmorillonite K10 catalyst. *Chem. Eng. J.* 165, 111–116. doi:10.1016/j.cej.2010.08.072

Djouonkep, L. D. W., Tamo, A. K., Doench, I., Selabi, N. B. S., Ilunga, E. M., Lenwoue, A. k., et al. (2022). Synthesis of high performance thiophene–aromatic polyesters from bio-sourced organic acids and polysaccharide-derived diol: characterization and degradability studies. *Mol* 27, 325. doi:10.3390/molecules27010325

Dong, H., Deng, J., Xie, Y., Zhang, C., Jiang, Z., Cheng, Y., et al. (2017). Stabilization of nanoscale zero-valent iron (nZVI) with modified biochar for Cr(VI) removal from aqueous solution. *J. Hazard. Mater.* 332, 79–86. doi:10.1016/j.jhazmat.2017.03.002

Dong, M., Zhou, H., Liu, W., and He, C. (2020). Activated carbon prepared from semi-coke as anEffective adsorbent for dyes. *Pol. J. Approx. Stud.* 29, 1137–1142. doi:10.15244/pjoes/101616

Du, J., Bao, J., Lu, C., and Werner, D. (2016). Reductive sequestration of chromate by hierarchical FeS@Fe0 particles. *Water Res.* 102, 73–81. doi:10.1016/j.watres.2016.06.009

Duarte, F. M., Maldonado-Hódar, F. J., and Madeira, L. M. (2013). Influence of the iron precursor in the preparation of heterogeneous Fe/activated carbon Fenton-like catalysts. *Appl. Catal. A General.* 458, 39–47. doi:10.1016/j.apcata.2013.03.030

Fletcher, A., Somorin, T., and Aladeokin, O. (2024). Production of high surface area activated carbon from peanut shell by chemical activation with zinc chloride: optimisation and characterization. *Bioenerg. Res.* 17, 467–478. doi:10.1007/s12155-023-10683-7

Gloria, M. (2010). Development of functionalized activated carbons for the degradation of dyes from textile industry effluents by the heterogeneous Fenton process.

Gomathi Devi, L., Girish Kumar, S., Mohan, K., and Munikrishnappa, C. (2008). "Photo degradation of methyl orange azo dye," in *Advanced Fenton Process uzing zero valent metallic iron: influence of various reaction parameters and its degradation mechanism*. doi:10.1016/j.jhazmat.2008.08.017

Hassan, H., and Hameed, B. H. (2011). Fenton-like oxidation of acid red 1 solutions using heterogeneous catalyst based on ball clay. *Int. J. Environ. Sci. Dev.* 2, 218–222. doi:10.7763/IJESD.2011.V2.127

Hua, Z., Ma, W., Bai, X., Feng, R., Yu, L., Zhang, X., et al. (2014). Heterogeneous Fenton degradation of bisphenol A catalyzed by efficient adsorptive Fe3O4/GO nanocomposites. *Environ. Sci. Pollut. Res.* 21, 7737–7745. doi:10.1007/s11356-014-2728-8

IUPAC (1985). IUPAC | international union of pure and applied chemistry. *Pure Appl. Chem.* 57, 603–619. doi:10.1351/pac198557040603

Jaafarzadeh, N., Kakavandi, B., Takdastan, A., Kalantary, R. R., Azizi, M., and Jorfi, S. (2015). Powder activatedcarbon/Fe3O4 hybrid composite asahighly efficient heterogeneous catalyst for Fenton oxidation of tetra cycline: degradation mechanism and kinetic. *Rsc Adv.* 5, 84718–84728. doi:10.1039/C5RA17953J

Jacques, M. B., Guy, N. P., Jules, M. L., Harlette, Z. P., Maffeu, E. J., Said, M., et al. (2023). *Removal of crystal violet by TiO_2* loaded alkali-activated carbon hybrid material from Raphia farinifera fruit kernels: surface chemistry, parameters and mechanisms. *Biomass Conv. Bioref.* doi:10.1007/s13399-023-04988-y

Joshi, S., Adhikari, M., Pokharel, B. P., and Pradhananga, R. R. (2012). Effects of activating agent on the activated carbon from lapsi seed stone. *Res. J. Chem. Sci.* 2, 80–86.

Kenda, G. T., Kouteu, P. A. N., Tchuifon, D. R. T., Fotsop, C. G., Bopda, A., Kuete, H. I. T., et al. (2023). Green synthesis of magnetic biochars derived from biobased orange peel materials as sustainable heterogeneous catalytic supports for the fenton process. *Ara. J. Chem.* 17, 105502. doi:10.1016/j.arabjc.2023.105502

Khelifi, S., Ayari, F., Hassan, C. D., Chehimi, D. B., and Trablsi-Ayadi, M. (2016). Synthesis and characterization of heterogeneous catalysts and comparaison to iron-ore. *J. Chem. Eng. Process Technol.* 7, 316. doi:10.4172/2157-7048.1000316

Kimouche, K. (2008). Study of some experimental designs associated with response surfaces [Doctoral thesis Mentouri Constantine Univ.]. doi:10.1155/2008/14541

Kouotou, D., Ghalit, M., Ndi, J. N., Martinez, L. M. P., Ouahabi, M. E., Ketcha, J. M., et al. (2021). *Removal of metallic trace elements (Pb^{2+}, Cd^{2+}, Cu^{2+}, and Ni^{2}+) from* aqueous solution by adsorption onto cerium oxide modified activated carbon. *Environ.Monitoring Assess.* 193 (8), 467. doi:10.1007/s10661-021-09267-9

Kpinsoton, G. M. R. (2019). *Elaboration des catalyseurs à base de charbons actifs et de latérites pour la dégradation du bleu de méthylène par procédé fenton hétérogène, Thèse de Doctorat/Ph.D., Institut 2IE, Ouagadougou, Burkina Faso*, 179.

Kuete, T. I. H., Tchuifon, T. D. R., Doungmo, G., and Anagho, S. G. (2018). *Preparation and Characterization of activated Carbons from bitter kola (Garcinia kola) nut Shells by chemical activation method using H_3PO_4; KOH and $ZnCl_2$. Chem.l Sci. Int. J.* 23 (4), 1–15. doi:10.9734/csji/2018/43411

Lall, A., Kamdem Tamo, A., Doench, I., David, L., Nunes de Oliveira, P., Gorzelanny, C., et al. (2020). Nanoparticles and colloidal hydrogels of chitosan-caseinate polyelectrolyte complexes for drug-controlled release applications. *Int. J.Mol. Sci.* 21, 5602. doi:10.3390/ijms21165602

Li, S., Xu, S., Liu, S., Yang, C., and Lu, Q. (2004). Fast pyrolysis of biomass in free-fall reactor for hydrogen-rich gas. *Fuel Process. Tech.* 85, 1201–1211. doi:10.1016/j.fuproc.2003.11.043

Mafo, S. G., Tchuifon, D. R., Ngakou, C. S., Fotsop, C. G., Kouteu, P. A., Doungmo, G., et al. (2023). Study of the degradation of Bezaktiv Brilliant Blue by the Fenton process using a prepared ferromagnetic activated carbon from rubber seed hull as heterogeneous catalyst. *Desalin. Water Treat.* 2023, 1–14. doi:10.5004/dwt.2023.29358

Mazilu, I., Ciotonea, C., Chirieac, A., Dragoi, B., Catrinescu, C., Ungureanu, A., et al. (2017). Synthesis of highly dispersed iron species within mesoporous (Al-) SBA-15 silica as efficient heterogeneous Fenton-type catalysts. *Microporous Mesoporous Mater* 241, 326–337. doi:10.1016/j.micromeso.2016.12.024

Muhammad, A., and Mashi, A. L. (2020). Application of central Composite design to the photo Fenton degradation of methyl orange azo dye using Fe-activated carbon catalyst. *Int. J. Innov. Sci. Res. Technol.* 5 (8), 479–485. doi:10.38124/IJISRT20AUG449

Ndi, J. S., Ketcha, J. M., Anagho, S. G., Ghogomu, J. N., and Bilibi, E. P. D. (2014). Physical and chemical characteristics of activated carbon prepared by pyrolysis of chemically treated cola nut (cola acuminata) shells wastes and its ability to adsorb organics. *Int. J. Adv.Chem. Techno.* 3, 1–13. doi:10.4236/ojic.2021.111001

Ndifor-Angwafor, G. N., Bopda, A., Tchuifon, T. D. R., Ngakou, S. C., Kuete, T. I. H., and Anagho, S. G. (2017). Removal of paracetamol from aqueous solution by adsorption onto activated carbon prepared from rice husk. *J. Chem. Pharm. Res.* 9 (3), 56–68.

Ngakou, C. S., Ngomo, H. M., Tchuifon, T. D. R., and Anagho, S. G. (2017). Optimisation of activated carbon preparation by chemical activation of ayous sawdust, cucurbitaceae peelings and hen egg shells using response surface methodology. *Int. Res. J. Pure Appl. Chem.* 14 (4), 1–12. doi:10.9734/IRJPAC/2017/38021

Ngankam, S., Lemankreo, D., Baissassou, D., Abdellaziz, B., Abdelrani, Y., and Abdoul, N. (2020). Preparation and characterization of magnetic banana peels biochar for fenton degradation of methylene blue. *Mater. Sci. appli.* 11, 382–400. doi:10.4236/msa.2020.116026

Ngeno, E., Mbuci, E., Necibi, M., Shikuku, V. O., Olisah, C., Ongulu, R., et al. (2022). Sustainable re-utilization of waste materials as adsorbents for water and wastewater treatment in Africa: recent studies, research gaps, and way forward for emerging economies. *Environ. Adv.* 9, 100282. doi:10.1016/j.envadv.2022.100282

Ngueabouo, A. M. S., Tagne, R. F. T., Tchuifon, D. R. T., Fotsop, C. G., Tamo, A. K., and Anagho, S. G. (2022). Strategy for optimizing the synthesis and characterization of activated carbons obtained by chemical activation of coffee husk. *Mater. Adv.* 3, 8361–8374. doi:10.1039/d2ma00591c

Njewa, J. B., and Shikuku, V. O. (2023). Recent advances and issues in the application of activated carbon for water treatment in Africa: a systematic review (2007–2022). *Appl. Surf. Sci. Adv.* 18, 100501. doi:10.1016/j.apsadv.2023.100501

Okieimen, F. E., Okiemen, C. O., and Wuana, R. A. (2007). Preparation and characterization of activated carbon from rice husks. *J. Chem. Soc.* 32, 126–136. doi:10.1155/2022/9975444

Peng, Z., Fan, Z., Chen, X., Zhou, X., Gao, Z. F., Deng, S., et al. (2022). Fabrication of nano iron oxide-modified biochar from Co-hydrothermal carbonization of microalgae and Fe(II) salt for efficient removal of rhodamine B. *Nanomaterials* 12, 2271. doi:10.3390/nano12132271

Ramirez, J. H., Maldonado-Hódar, F. J., Pérez-Cadenas, A. F., Moreno-Castilla, C., Costa, C. A., and Madeira, L. M. (2007). Azo-dye Orange II degradation by heterogeneous Fenton like reaction using carbon-Fe catalysts. *Appl. Catal. B Environ.* 75, 312–323. doi:10.1016/j.apcatb.2007.05003

Sahira, J., and Bhadra, P. P. (2014). Preparation and characterization of activated carbon from lapsi (choerospondias axillaris) seed stone by chemical activation with potassium hydroxide. *J. Inst. Eng.* 9 (1), 79–88. doi:10.3126/jie.v9i1.10673

Sandrale, G. M. M., Donald, R. T., Christian, S. N., and Cyrille, G. F. (2023). Study of the degradation of Bezaktiv Brillant Blue by the Fenton process using a prepared ferromagnetic activated carbon fron rubber seed hull as heterogeneous catalyst. doi:10.5004/dwt.2023.29358

Shikuku, V. O., Renato, Z., Kowenje, C. O., Donato, F. F., Bandeira, N. M. G., and Prestes, O. D. (2018). Single and binary adsorption of sulfonamide antibiotics onto iron-modified clay: linear and nonlinear isotherms, kinetics, thermodynamics, and mechanistic studies. *Appl;Water Sci.* 8, 175. doi:10.1007/s13201-018-0825-4

Sidjou, A. S., Tchakounte, A. N., Shikuku, V., Lenou, I., Djimtibaye, R., and Dika, M. M. (2023). Synthesis of alkali-activated volcanic scoria and rice husk ash based composite materials for adsorptive removal of crystal violet: optimization, kinetics, isotherms and mechanism. *Hybrid. Adv.* 4, 100113. doi:10.1016/j.hybadv.2023.100113

Taquieteu, I. K., Tamaguelon, H. D., Shikuku, V., Banenzoué, C., and Dina, D. J. (2023). Fixed-bed adsorption of an azo dye (methyl orange) onto chemically and thermally regenerated activated carbons. *J. Chem.* 2023, 1–15. doi:10.1155/2023/6677710

Tchuifon, T. D. R., Anagho, S. G., Ketcha, J. M., Ndifor-Angwafor, G. N., and Ndi, J. N. (2014). Kinetics and equilibrium studies of adsorption of phenol in aqueous solution onto activated carbon prepared from rice and coffee husks. *Int. J. Eng. Tech. Res.* 2, 166–173. doi:10.4236/gep.2014.1007

Varjani, S. J., and Sudha, M. C. (2018). "Treatment Technologies for emerging organic contaminants removal from wastewater," in *Water remediation* (Singapore: Springer Nature), 91–115. doi:10.1007/978-981-10-7551-3-6

Wang, S., Nam, H., and Nam, H. (2020). Preparation of activated carbon from peanut shell with KOH activation and its application for H2S adsorption in confined space. *J. Environ. Chem. Eng.* 8 (2), 103683. doi:10.1016/j.jece.2020.103683

Yang, H.He S., Daqing, W., Dong, C., Liang, X., Qin, Z. M., Fan, J., et al. (2009). Decolorization of methylene blue by heterogeneous Fenton reaction using Fe3xTixO4(0x 0.78) at neutral pH values. *Appl. Catal. B Environ.* 89, 527–535. doi:10.1016/j.apcatb.2009.01.012

Yao, Y., Wang, L., Sun, L., Zhu, S., Huang, Z., Mao, Y., et al. (2013). Efficient removal of dyes using heterogeneous Fenton catalysts based on activated carbon fibers with enhanced activity. *Chem. Eng. Sci.* 101, 424–431. doi:10.1016/j.ces.2013.06.009

Zhang, G., Qu, J., Lui, H., Cooper, A. T., and Wu, R. (2007). *$CuFe_2O_4$*/activated carbon composite; a novel magnetic adsorbent for the removal acid orange II and catalytic regeneration. *Chemosphere* 73, 1524–1528. doi:10.1016/j.chemosphere.2007.07.081

Zhou, W., Rajic, L., Chen, L., Kou, K., Ding, Y., Meng, X., et al. (2019). *Activated Carbon as effective cathode Material in iron-free electro-fenton process: integrated H_2O_2* electrogeneration, activation, and pollutants adsorption. *Electrochem. Acta.* 296, 317–326. doi:10.1016/j.electacta.2018.11.052